Performance of a Position Sensitive Neutron Scintillation Detector based on Silicon Photomultipliers

S. Kumar, *Student Member, IEEE,* M. Herzkamp, C. Degenhardt, J. Seemann, E. Vezhlev, S. van Waasen

[1] *Abstract*– **In recent years, the price increase of ³He has triggered the search for alternative neutron detectors. One of the viable options is a scintillation based neutron detector. Usually, Photomultiplier tubes (PMTs) are used in these detectors for photodetection. However, the increase in performance requirements such as the operability in magnetic field and spatial resolution, necessitates an advanced neutron detector. Therefore, we developed a detector prototype with an active area of 13 cm × 13 cm using Silicon photomultipliers (SiPM). As compared to PMTs, SiPMs offer more compactness, more robustness and a lower sensitivity to magnetic fields. The final detector is aimed to be used in the future at the *TREFF* instrument of the *Heinz Maier-Leibnitz Zentrum (MLZ)* in Garching, Germany for neutron reflectometry (NR). First measurements were carried out at *TREFF* and at the dedicated detector test instrument *V17* at *BER-II* of *HZB* in Berlin, Germany. In this work, we report the results for detection efficiency, gamma discrimination, two-dimensional position resolution, count rate, and detection linearity.**

I. Introduction

The demand for a thermal neutron detector as an alternative to ³He tubes is growing due to the rise in price for ³He in 2009 [1]. Detectors based on a scintillation process can be a prominent substitute [2]. Thus, we developed an advanced neutron detector based on the *Anger camera* [3] approach, using ⁶Li glass scintillators, which offers high spatial resolution, a scalable detection area, a high detection efficiency, and a high count rate capability. Usually, PMTs are used as photodetectors in two-dimensional position sensitive neutron detectors (PSND) [4] [5] [6]. Nonetheless, the electro-mechanical complexity associated with their development, high sensitivity to magnetic fields, high voltage requirements (few kV), and low (~30%) photon detection efficiency (PDE) limits the usability of these PSNDs. Therefore, the scintillator detector prototype we built for detecting cold and thermal neutrons is based on a solid-state photodetector, namely Silicon photomultipliers (SiPM) [7]. The SiPM has better performance characteristics than PMTs such as a lower operating voltage (~25V), a higher PDE (~50%) and an insusceptibility to magnetic fields.

Concerning radiation hardness of SiPMs in cold/thermal neutron detection, our investigation shows that SiPMs have an expected life time of 10 years of operation with an acceptable performance degradation for typical Small Angle Neutron Scattering experiments [8] [9]. Hence, SiPMs can be a possible alternative to PMTs for such applications [10].

We tested our detector prototype with cold (λ = 5Å) and thermal neutrons (λ = 3.35Å) at two research reactors: FRM-II and BER-II in order to evaluate the detector efficiency, gamma discrimination, spatial resolution, count rate, and linearity. Due to technical problems, measurements at FRM-II were not successful, and only some intermediate measurements were performed. The beamline at the V17 instrument at BER -II is monochromatized by a pyrolythic graphite crystal. The beam wavelength was calculated according to Bragg's law using crystal thickness (4 mm), crystal area (8 x 1 cm²), knowing the lattice constant of the material, and measuring the take-off angle (60°). No filter, however, was used to get rid of higher harmonics, so it is possible that the beam was "contaminated" by neutrons of the half wavelength (1.68 Å).

II. Detector

The detector (Fig. 1) with an active area of 136.5 mm × 136.5 mm, has three major subassemblies: (1) optical front-end, (2) readout electronics, and (3) the cooling system (Fig. 2). We used 1mm thick *GS20®* [11], a ⁶Li-enriched Cerium-doped monolithic glass scintillator, a light guide, and four digital SiPM modules [12] for the front end. Each module consists of 2 × 2 "tiles" and a tile is an array of 4 × 4 "dies". A die is an
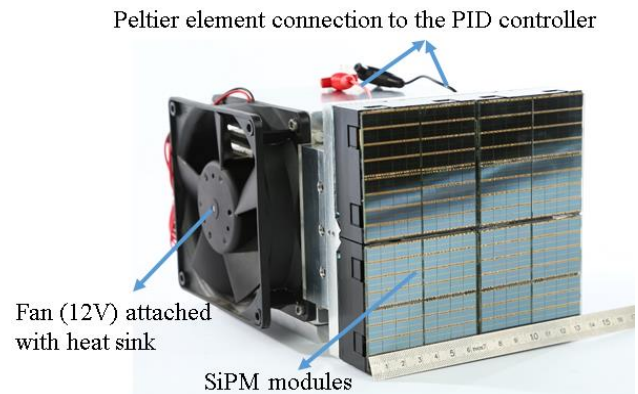
Fig. 1: Side view of the detector. The four SiPM modules from Philips, data transmission cable and cooling system are visible in the picture.

[1]Manuscript submitted on Dec 25, 2019.
   S. Kumar, M. Herzkamp, C. Degenhardt, J. Seemann and S. van Waasen are with Central Institute of Engineering, Electronics and Analytics ZEA-2 – Electronic Systems, Forschungszentrum Jülich GmbH, 52425 Jülich, Germany (telephone: 2461-61-85120, e-mail: s.kumar @fz-juelich.de). S. van Waasen is also with Faculty of Engineering, Communication Systems (NTS), University of Duisburg-Essen, 47057 Duisburg, Germany.
   E. Vezhlev is with Jülich Centre for Neutron Science (JCNS-4) at Heinz Maier-Leibnitz Zentrum (MLZ), Forschungszentrum Jülich GmbH, 85748 Garching, Germany.
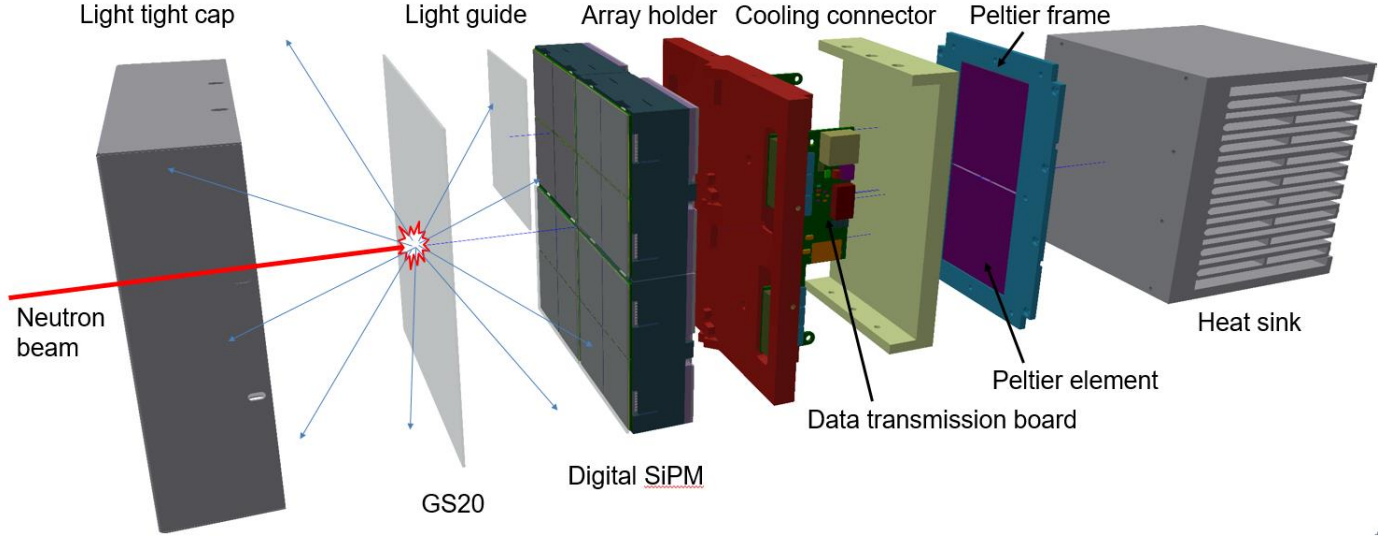
Fig. 2: Exploded view of the detector. (color online)

independent detection unit, which comprises 2 × 2 "pixels" (a single SiPM) and further, a pixel is subdivided into 4 subpixel. For the light guide, we employed a borosilicate thin (1.1 mm) glass manufactured by *SCHOTT* [13]. The detailed description of the optical front-end design can be found be in [14].
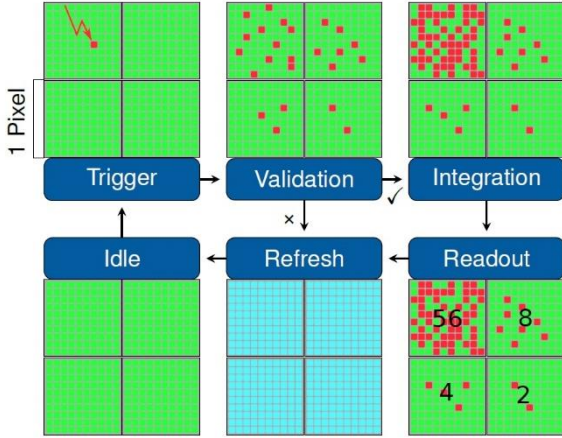

Fig. 3: Schematic of the readout cycle of SiPM utilized for this work. The photon event acquisition starts once the trigger logic is fulfilled, then it checks for a validation scheme and, if satisfied, moves to next step of integration to finally start the readout. The trigger scheme, as well as the validation and integration times are configurable and the numbers represented here are only for visualization. (color online)

The readout mechanism is comprised of three sub-systems. The first sub-system is the sensor chip itself that contains a detection unit, the readout circuits and the time-to-digital converter (TDC), which generates a digital signal. The readout cycle (see Fig. 3) of the sensor incorporates the trigger scheme, as well as the validation, integration, and readout intervals, respectively. The event based acquisition sequence starts with a trigger signal once the trigger scheme was set ("single" or "multiple" triggered cells options, where the triggering is initiated only if there is a triggered cell in only one, two, three or all four of the so called "sub-pixels" logically connected within each SiPM simultaneously) and its triggering condition is fulfilled. This means the acquisition sequence will be started only by those

dies that detect sufficient photons to reach the configured thresholds. For the present work, the trigger scheme chosen was 4, which implies that there should be at least one fired cell in all 4 subpixels and on average, 8 photons needed to initiate the readout cycle. Discrimination between avalanche events, triggered either by the thermally generated electrons (dark counts or noise), by crosstalk, after-pulsing, and impinging visible photons emitted by the absorption of a neutron in the scintillation glass, is performed during the so called "validation interval" of 35 ns. If the event is validated, it enters the "integration phase" of 165 ns to accumulate further photons belonging to the same event. Afterwards, the die counts the number of triggered cells in each pixel and stores these numbers along with the timestamps of each detected photon in a local buffer. The duration of the "readout phase" is 680 ns. Finally, the cells are recharged and ready to receive the next event. In the second sub-system, the digital information from the sensor is forwarded with a maximum data rate of ~20 Mbps per tile to a PCB. Two SiPM modules at a time are connected to the PCB, which forwards this data to a "concentrator" PCB (third sub-system) via an HDMI cable and provides power and clock to the modules. This PCB which contains a FPGA module is responsible for collecting the data of all four modules, and sending it to an external PC via USB 3.0, where neutron positions are reconstructed.

As it is a well-known fact that the SiPM has a strongly temperature dependent performance due to the noise fluctuation with temperature variation, a cooling system consisting of Peltier elements, a heat sink, and a fan were utilized to keep the temperature around 21 °C. Fig. 4 shows the variation in temperature during one of the performed experiments. Although it would have been an interesting measurement to observe the behavior of the detector over a temperature range, we refrained from it due to the measurement complexity, but might attempt it in the near future.

III. POSITION RECONSTRUCTION

The position reconstruction algorithm we employed was based on simulation data. We estimated the neutron position by comparing the number of photon counts detected by the SiPM
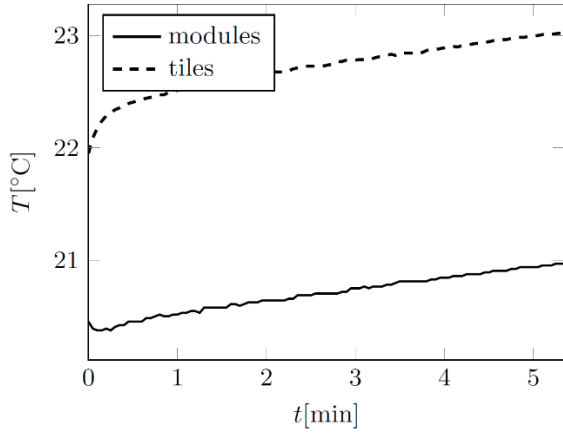
Fig. 4: Plot for the temperature variation within a tile and module recorded by the detector during a five minute measurement. The temperature sensor was directly placed behind a module.

Fig. 5: Graph showing the measurement results for the maximum brightness ratio against the sum of triggered cells. (color online)

to the theoretically expected photon counts obtained from the simulation. In order to establish confidence in the validity of our simulation data, we compared the distribution of photons across the SiPM pixels. As we cannot measure the photon distribution directly, we used the maximum brightness ratio (brightest pixel response in an event divided by the sum of all pixel responses) plotted against the sum of all pixel responses in one event. The data for the plot shown in Fig. 5 was obtained from the measurement performed at FRM-II. The maximum brightness ratio from the simulation data is shown in Fig. 6. The close resemblance of the shapes of both plots suggests that most physical aspects are captured in our simulations. The number of events with more than 900 triggered cells in the measurement are likely events with multiple neutrons and associated higher photon count. In our simulations we analyzed every neutron event separately and therefore could not get multi-events. Various other validation measurements of the simulations have been performed at BER-II and are described in [15]. All other measurements reported here were carried out at BER-II.

We implemented a least square deviation minimization algorithm, where the measured photon counts c_i were compared with expected photon counts $\langle n_i \rangle_{(x,y)}$ obtained from the simulation using the Geant4 tool-kit [16]. Utilizing the photon distribution obtained on the sensor for a large set of neutron events at the same position, look-up tables (LUT) were created to obtain the light response function (LRF) (see Fig. 7). The LRF was optimized by tuning the light guide thickness, the photon detection efficiency, and the dark count rate of the SiPM.

In order to increase the performance of our reconstruction algorithm, we divided the 136.5 mm side length into 1024 channels and considered only points (x_m, y_m) on the resulting mesh for minimization of the function W.

$$W = \sum \frac{\left(\langle n_i \rangle_{(x_m, y_m)} - c_i\right)^2}{\langle n_i \rangle_{(x_m, y_m)}}$$

For the minimization we used the discrete Steepest Descent algorithm with the center of gravity serving as the starting point.
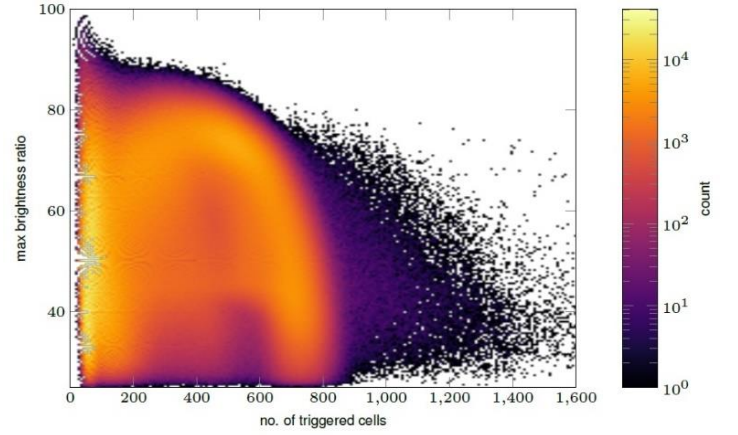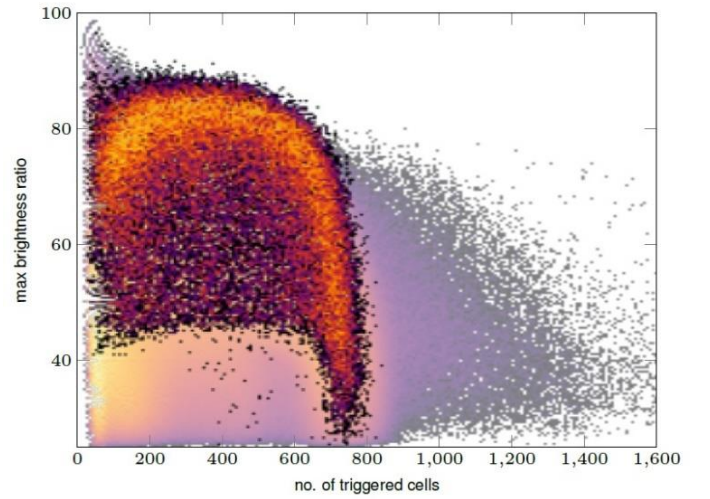

Fig. 6: Comparison of measurement and simulation for the maximum brightness ratio response to the triggered cells, depicting a good match between them. The color scale is same as the one in Fig. 5. (color online)
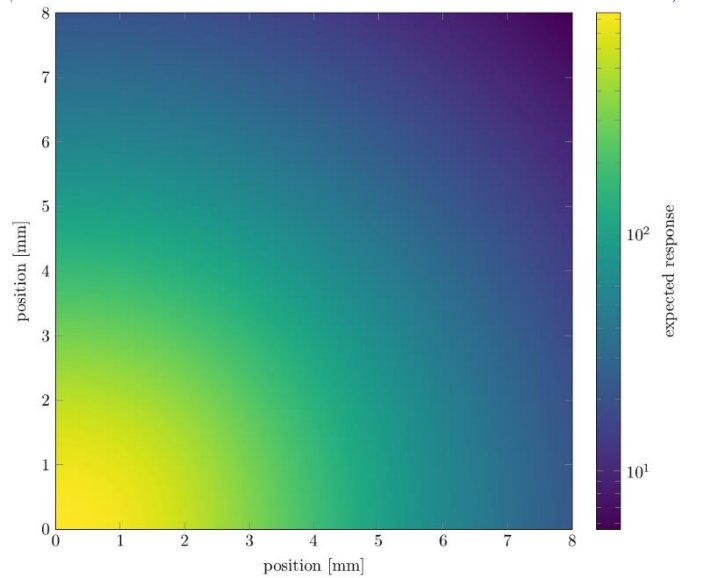

Fig. 7: Example of a pixel look up table, created within 8 mm × 8 mm for pixel at (0, 0) and neutron event at (x, y) using the simulation data. (color online)

IV. Measurements and Results

In order to validate the simulation and characterize the detector, we conducted several measurements. We determined the detection efficiency by comparing the number of events measured by our detector with a high pressure ^{3}He tube during a 3 minute measurement of a 3.35 Å neutron beam with a 20×2 mm aperture (Fig. 8). During the helium tube measurement, we used our detector in order to make sure that the beam intensity was reduced to zero by the tube, capturing all neutrons. This implies that no counts were registered by the detector when the ^{3}He tube was placed in the beam in front of the detector after which the tube was removed from the beam to allow the detector to count (see Fig. 9). Thus, we assumed a 100 % efficiency rate for ^{3}He tube. The helium tube counted 560880 events within 3 minutes, while our detector measured 537406 neutrons. As such, our detector showed a detection efficiency of 96 ± .13 %. It should be noted that this value correspond to that particular region only and is the maximum efficiency achieved by the detector. This value varies across the surface, due to the detector structure, and can be adjusted by different threshold setting.

The linearity was determined by comparing the detector's response to differently attenuated beams to the response of a fission chamber in the same beam. The fission chamber from *LND INC.* [17] has ^{235}U (cross section of ~500 barn) as the neutron sensitive material and filled with Ar and N gases. For this measurement, we used a 20 mm × 20 mm aperture, which resulted in a 570 mm^2 irradiated area on the detector surface. Fig. 10 shows that the responses are proportional up until the highest intensity measurement, which resulted in 186 million counts in 5 minutes. Therefore, 1.09 kcps/mm^2 is a lower bound for the detection rate at which our detector still operates linearly.

We examined the position resolution of our detector by placing boron carbide masks (see Fig. 11) with structures (circular and rectangular) ranging from 0.5 mm to 4 mm in front of the detector surface and determining the visibility of these structures in the reconstructed images. Fig. 12 shows the reconstructed image of such a mask, completely illuminated by a broad neutron beam.
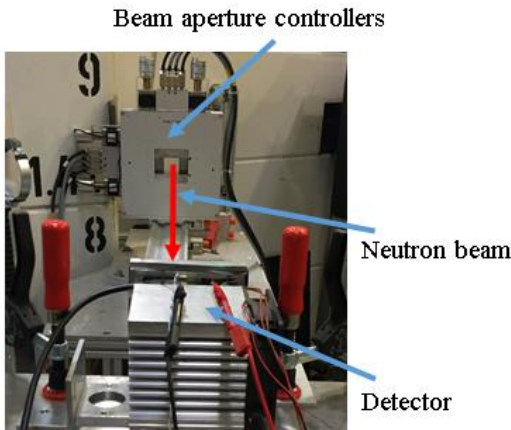

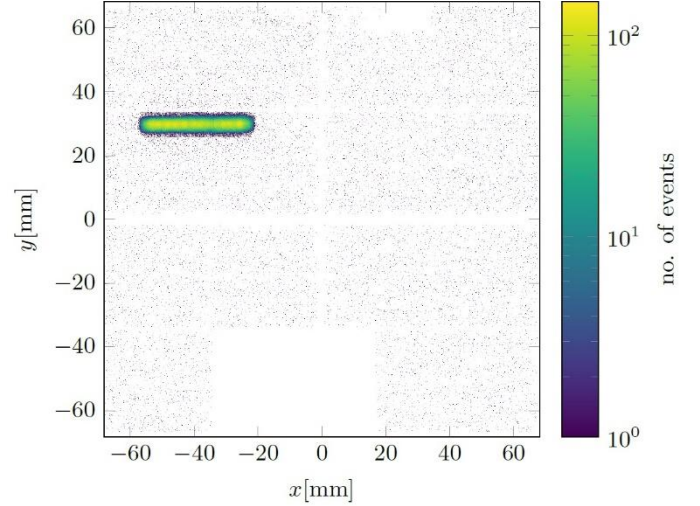*Fig. 9: Reconstructed image, as seen by the detector, for the efficiency measurement after the ^{3}He tube was removed. Certain area (bottom center) of the detector was offline and did not recorded any event. (color online)*
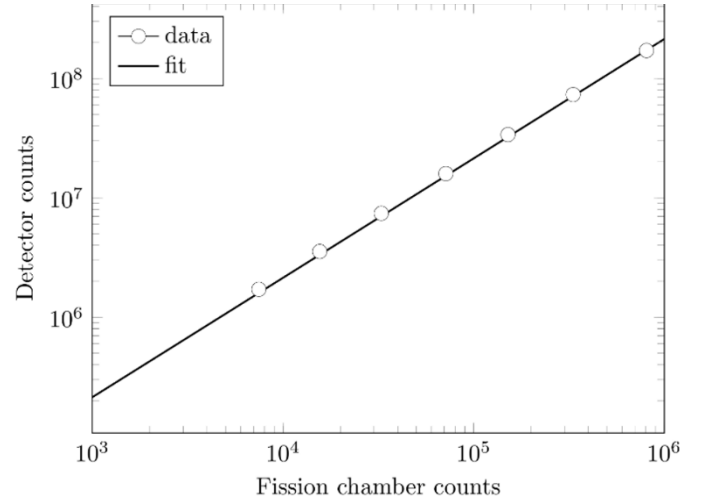

Fig. 10: Comparison between detector and fission chamber response at BER-II to different neutron beam intensities, including a linear fit.
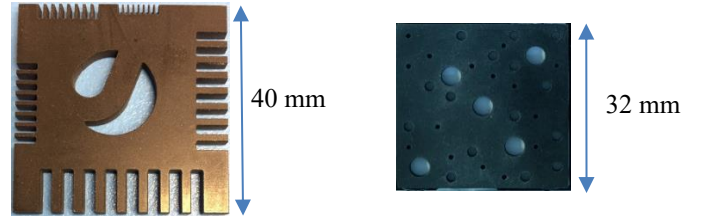

Fig. 11: Physical representation of B$_4$C mask used for mapping. The second mask having holes with a diameter from 1 mm up to 4 mm.

The 0.75 mm structure can be discerned easily, and even the 0.5 mm structure is resolved on the top right part in Fig. 12. Using multiple different mask positions (see Fig. 13), we conclude that the detector is able to resolve 1 mm structures anywhere on its active surface, except for the lines which form a cross at the detector's center in Fig. 12.
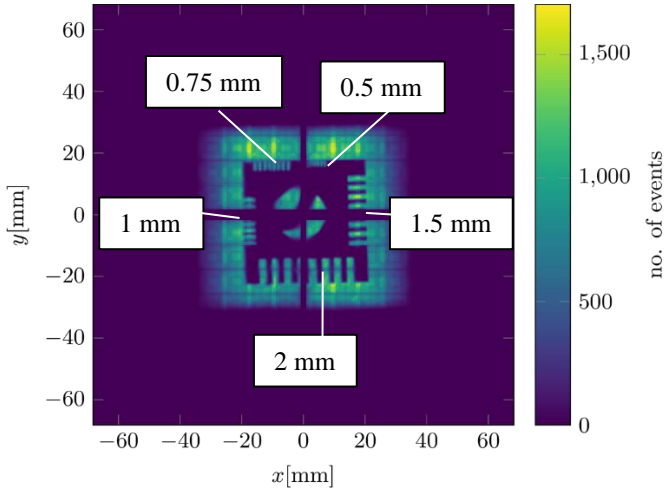

Fig. 8: Depiction of measurement set up at BER-II utilized to evaluate the detection efficiency relative to ^{3}He tube.

Fig. 12: Reconstructed image of a mask with structures ranging from 0.5 mm to 2 mm and the beam aperture measuring 40 × 40 mm. (color online)
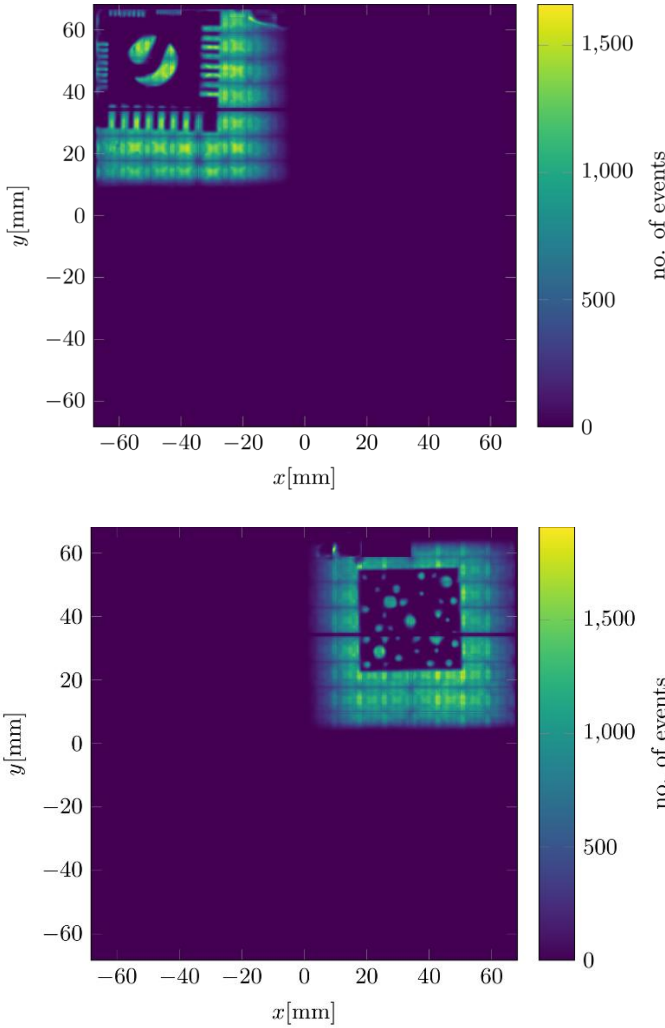

Fig. 13: Reconstructed image of masks at different positions with structures ranging from 0.5 mm to 4 mm and beam aperture 40 × 40 mm, measured at at BER-II. (color online)

These lines stem from the fact that we used 4 SiPM modules (*Philips Digital Photon Counters DPC-3200*) to cover the scintillator, which cannot be placed without dead space between them. This could be mitigated in future by using a dedicated fabrication of SiPM (PDPC) for the given application, or searching for other large area SiPM with minimal dead space arising due to integration. However, for the given application this was not a major concern for the development of this prototype. Additionally, it is worth mentioning that a structure pattern can be observed in the Fig. 12 & 13, mainly because of the variation in the detection efficiency across the detector. This might be attributed to the fact that the sensor was provided by the manufacturer with an anti-reflective glass coating having orientation alignment mismatch up to 0.4 mm across a tile surface. This leads to a non-uniform effective thickness of the light guide within a die and consequently to varying LUTs. Nevertheless, further investigation is needed to address thise structure pattern issue.

In order to quantify the detector's resolution, we measured its response to a 1 mm slit mask placed vertically in front of it. Fig. 14 shows the projection of the reconstructed image on the horizontal axis, as well as a fit of a 1 mm characteristic function with a Gaussian blur with standard deviation σ. The optimal fit results in $\sigma = 0.43$ mm, which translates to a FWHM of 1.01 mm for a point source.
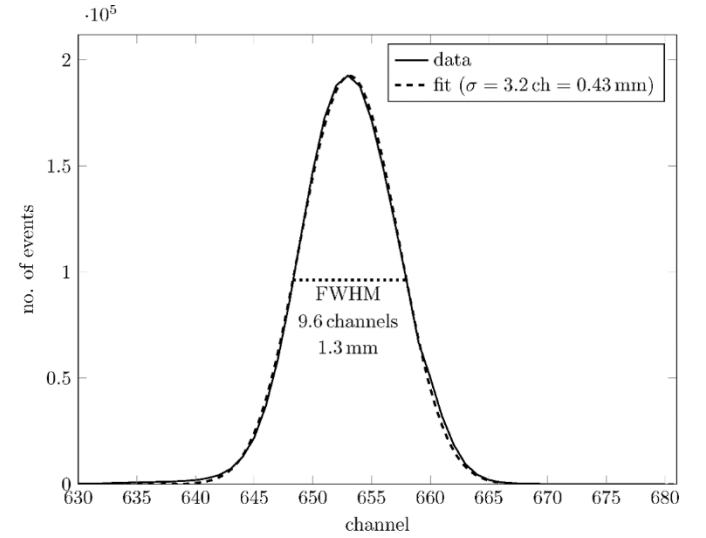

Fig. 14: Graph showing the projection of counts onto the x-Axis during irradiation through a 1 mm slit at BER-II. The data was fitted by a convolution of a Gaussian bell curve with a 1 mm rectangular function.

Although, the gamma discrimination was not the focus of the study, we roughly determined it by placing several gamma sources with known activity directly in front of the detector and performed the measurements. The number of detected events was compared to the expected number of incident gamma particles. We approximated the discrimination ratio using the following formula, and Table 1 shows the results of these measurements.

$$Discrimination\ ratio = \frac{detected\ events}{radioactivity * time * \gamma}$$

Isotope	Energy[MeV]	Activity[Bq]	Count rate[cps]	Discrimination factor
^{60}Co	1.17, 1.33	4.7×10^5	250	10^{-4}
^{137}Cs	0.662	1.9×10^6	2.1	10^{-6}
^{241}Am	0.059	1.7×10^6	0.2	10^{-7}

Table 1 The activities of sources and count rates measured when placing these sources directly in front of the detector. The values are an approximation as the same threshold setting were used for the neutron measurements.

The measurement settings were not altered, which was optimized for the neutron detection, so the results reported in the table are only valid for the actual setup and threshold setting. The response of the detector is based on pulse height not on pulse energy. This implies the energy spectrum at the detectors position was neither known nor measured, it reflects only the number of photons that were obtained from the detector. Therefore, the detector design, the scintillator, and the measurement settings used to limit the noise of the detector has contributed to those numbers in table 1.

V. Conclusion

We developed a scintillation neutron detector based on SiPMs for light detection and tested it at two neutron sources. The measurements show that the detector has a neutron detection efficiency of more than 95 % for cold neutrons, a linear count rate up to at least 1.09 kcps/mm^2, and a two-dimensional position resolution of 1 mm across the active surface.

Acknowledgment

References

[1] U.S. Government Accountability Office (GAO), *Technology Assessment: Neutron Detectors. Alternatives to using helium-3. Report to Congressional Requesters*, GAO- 11-753, 2011.

[2] Richard T. Kouzes *et al*., Neutron detection alternatives to 3He for national security applications, Nuclear Instruments and Methods in Physics Research A, vol. 623 (2010), p.1035-1045,

[3] H. O Anger, "Scintillation camera" Review of Scientific Instruments, Vol. 29, No. 1, 1958, p.27

[4] M. G Strauss, R. Brenner, F. J Lynch, C. B Morgan "2-D Position senstive scintillaion detector for neutrons" IEEE Transactions on Nuclear Science, Vol. 28, No. 1, 1981, p.800

[5] G. Kemmerling *et al*., "A new two-dimensional scintillation detector system for small-angle neutron scattering experiments," in *IEEE Transactions on Nuclear Science*, vol. 48, no. 4, pp. 1114-1117, Aug. 2001.

[6] P. M. De Lurgio *et al*., "2-D scintillation position-sensitive neutron detector," *IEEE Nuclear Science Symposium Conference Record, 2005*, Fajardo, 2005, pp. 648-653.

[7] D. Renker, Geiger-mode avalanche photodiodes, history, properties and problems, Nuclear Instruments and Methods in Physics Research A, vol.567 (2006), p. 48-56

[8] D. Durini *et al.* "Evaluation of the dark signal performance of different SiPM-technologies under irradiation with cold neutrons" Nuclear Instruments and Methods in Physics Research A, vol.835 (2016) , p. 99

[9] S. Kumar, D. Durini, C. Degenhardt, S. van Waasen "Photodetection characterization of SiPM technologies for their application in scintillator based neutron detectors" Journal of Instrumentation Vol. 13 (2018) C01042

[10] M. Herzkamp et al "Development and characterization of a 4×4 mm2 pixel neutron scintillation detector using digital SiPM" Journal of Instrumentation Vol. 12 (2017) C12001

[11] 6-lithium scintillator glass available at https://scintacor.com/products/6-lithium-glass/ (accessed on Dec, 2019)

[12] T. Frach, G. Prescher, C. Degenhardt, R. Gruyter, A. Schmitz, R. Ballizany "The digital silicon photomultiplier – principle of operation and intrinsic detector performance" Proc. IEEE Nuclear Science Symposium Conference, Orlando, Florida 2009, pp. 1959–1965.

[13] Thin glass available at https://www.pgo-online.com/intl/D263.html (accessed on Dec, 2019)

[14] S. Kumar, M. Herzkamp, S. van Waasen , "Development of a solid-state position sensitive Neutron detector prototype based on Li-glass scintillator and digital SiPM arrays" Nuclear Instruments and Methods in Physics Research A, 2020, 954, 161697

[15] S. Kumar, M. Herzkamp, S. van Waasen, "Silicon photomultipliers based neutron detector design: validation of Geant4 simulations," Proc. SPIE 11114, Hard X-Ray, Gamma-Ray, and Neutron Detector Physics XXI, 111140R (9 September 2019); https://doi.org/10.1117/12.2526879

[16] S. Agostinelli et al "GEANT4- a simulation toolkit" Nuclear Instruments and Methods in Physics Research A 506 (2003) , p.50

[17] Fission chambers for neutron detectors available at https://www.lndinc.com/products/neutron-detectors/fission-chambers/3003 (accessed on Dec 2019).